Salmon Calcitonin and Amyloid β: Two Peptides with Amyloidogenic Capacity Adopt Different Conformational Manifolds in Their Unfolded States†

Reinhard Schweitzer-Stenner,*,‡ Thomas Measey,‡ Andrew Hagarman,‡ Fatma Eker,§ and Kai Griebenow§

Department of Chemistry, Drexel University, 32nd and Chestnut Streets, Philadelphia, Pennsylvania 19104, and Department of Chemistry, University of Puerto Rico, Río Piedras Campus, Post Office Box 23346, San Juan, Puerto Rico 00931

Received November 7, 2005; Revised Manuscript Received January 6, 2006

ABSTRACT: The molecular conformations of salmon calcitonin in aqueous solution have been investigated by exploiting the different influences of excitonic coupling on the amide I band profile in the isotropic and anisotropic Raman, FTIR, and vibrational circular dichroism spectra of a polypeptide. The N-terminal loop, caused by a disulfide bridge between cysteines at positions 1 and 7, was modeled by performing a conformational search by molecular mechanics calculations. The remaining part of the peptide chain was modeled as a mixture of three sequences containing different fractions of residues adopting poly-L-proline II (PPII), extended β-strand, and α-helix-like conformations. This yielded an excellent reproduction of the experimentally observed amide I′ band profiles. A comparison with recent data on the β-amyloid fragment Aβ_{1-28} revealed a lower PPII content and more conformational heterogeneity for calcitonin. Thus, our results underscore the notion that individual structural propensities of amino acid residues give rise to structural differences between the unfolded states of even long peptide chains, at variance with expectations based on a random or statistical coil model.

One of the basic textbook doctrines of protein chemistry is that the amino acid sequence of a polypeptide polymer is the key determinant of the three-dimensional structure, which is a prerequisite for protein function (*1*). However, this view is at variance with the experimentally established fact that nature has produced numerous so-called disordered or unfolded proteins with very well-defined functions (*2*, *3*). They have been found to be involved in the DNA/RNA−protein interaction, to function as inhibitors and scavengers, and also to facilitate in the formation and function of multiprotein complexes (*2*). Some of the thus far identified proteins/peptides such as the tau protein, α-synuclein, and the β-amyloid peptide Aβ_{1-42} are of particular biomedical relevance owing to their involvement in the development of neurodegenerative disorders (*4*−*7*).

In what follows, a rather rigid definition of the unfolded state is used in this paper, which excludes any of the classical structure motifs such as α_R, α_L, 3_{10}-helices, turns, hairpins, and β-sheets, thus following the recently adopted concept of Jha et al. (*8*). The formation of any of these conformations is considered as (local) folding. Now, the question arising from the above findings is how a protein can have a well-defined function even if it is structurally random. To address this issue, varying understandings of the term "random" have to be differentiated. The term random generally implies that every amino acid residue can sample the entire allowed region of the Ramachandran space, which is thus regarded as nearly ergodic. The energy differences between different backbone conformations should be small, e.g., in the order of RT (*9*, *10*). In this case, the end to end distance of a polypeptide is expected to exhibit a Gaussian distribution (*9*, *11*). The statistical coil model, however, allows a restriction of the conformational space sampled by the individual residues but still considers each residue as an entity independent of the structure of its neighbors (isolated pair hypothesis) (*9*). In this case, individual residues might adopt a limited number of conformations, but this structural preference does not prevent long peptides from being essentially coiled because the formation of substantial persistence lengths is disfavored by combinatorial entropy (*12*, *13*). However, if a significant number of residues have a strong preference for a single conformation and if nearest neighbor, nonlocal, and residue−solvent interactions favor the formation of a significant persistence length for this particular conformation, a long peptide can exhibit substantial nonrandom behavior.

The debate about the "random-coil state" started with the discovery by Tiffany and Krimm that the circular dichroism (CD) spectra of so-called random-coil peptides resemble that of *trans*-polyproline, which is known to adopt a poly-L-proline II (PPII)[1] conformation (*14*). This led them to conclude that peptides as well as proteins are able to locally

† Financial support was provided from the NIH−COBRE II Grant for the Center for Research in Protein Structure, Function, and Dynamics (P20 RR16439-01), from the NIH−SCORE Grant (S06 GM008102), and from the National Science Foundation (MCB-0318749).

* To whom correspondence should be addressed: Department of Chemistry, Drexel University, 32nd and Chestnut Streets, Philadelphia, PA 19104. Telephone: (215) 895-2268. Fax: (215) 895-1265. E-mail: rschweitzer-stenner@drexel.edu.

‡ Drexel University.

§ University of Puerto Rico.

[1] Abbreviations: sCT, salmon calcitonin; VCD, vibrational circular dichroism; PPII, poly-L-proline II; MD, molecular dynamics; DFT, Density Functional Theory.

10.1021/bi052282r CCC: $33.50
Published on Web 02/07/2006

adopt a PPII conformation. This notion was later confirmed by vibrational circular dichroism (VCD) studies on a variety of unfolded polypeptides and proteins (*15*, *16*). PPII is in fact a rather ordered structural motif, in that it exhibits a perfect 3-fold rotational symmetry for its canonical conformation with $(\phi, \psi) = (-78°, 146°)$ (*17*). The PPII signal was observed in the spectrum of the unfolded state of many proteins subjected to denaturing detergents (*18*). ECD (electronic circular dichroism) and Raman optical activity (ROA) spectra of the tau protein, casein, stathmin, and Bob1 suggest that their structure contains a substantial amount of PPII (*19*−*21*). This seems to imply that the term "intrinsically unstructured proteins" is, in principle, inappropriate (*22*).

Over the last 5 years, a variety of experimental and theoretical studies have provided considerable evidence for conformational propensities of individual amino acid residues in short unfolded peptides (*8*, *12*, *23*−*29*). A significant PPII propensity was obtained for residues with alanine, lysine, glutamate, and glutamic acid side chains (*22*−*25*, *27*, *30*, *31*), while valine, isoleucine, and phenylalanine were found to prefer a more extended, β-strand-like conformation (*24*, *25*, *29*, *30*). While these findings are at variance with the conventional notion that the conformation of short peptides is random (*32*−*34*), they do not, per se, imply that the unfolded state of long peptides and even proteins are nonrandom. Tran et al. recently showed that a rather simple molecular model, which describes a peptide in a good solvent by solely invoking interatomic-excluded volume interactions, yields different structural preferences for individual amino acid side chains and a statistical coil behavior for long chains (*12*). Their finding seems to reconcile the experimentally verified individual propensity with another experimental observation, namely, that the length dependence of the radius of gyration of a large number of polypeptides was found to be practically independent of the respective amino acid sequence (*35*). Although intrinsically convincing and consistent, it cannot be overlooked that the results of Tran et al. (*12*) do not account for some recently reported experimental results. First, they cannot explain the experimental observation that the PPII propensity of alanine peptides increases with the number of residues (*36*, *37*), the occurrence of PPII helices of 4−6 residues in a 28-residue PEVK module of human fetal titin (*38*), the obtained context dependence of PPII propensity of alanine (*27*), and most importantly, the weak but significant cooperativity of PII $\leftrightarrow$ β and PPII $\leftrightarrow$ random-coil transition of the amyloid Aβ_{1-40} peptide and some of its fragments recently reported by Gräslund and associates (*39*). Second, the individual propensities predicted by Tran et al. (*12*) do not reproduce the high PPII propensity of ionized glutamic acid and lysine and the high β-strand propensity of valine inferred from spectroscopic investigations of tripeptides (*26*). Interestingly, recent molecular dynamics (MD) calculations by Garcia (*40*), Kentsis et al. (*41*), Mezei et al. (*42*), and Fleming et al. (*43*) clearly indicated that the aqueous environment can stabilize a significant persistence length of PPII in polyalanine peptides. If this is indeed the case, the unfolded state cannot be described by a random coil.

In this context, it is of interest to investigate longer peptides that do not fold into one of the classical secondary structures in water. A classical example is the amyloid peptide A$\beta_{1-41(42)}$, which is most likely responsible for Alzheimer's disease (*4*). In its monomeric state, it appears unfolded in water in the absence of any reagents that support the formation of α-helical segments. This unfolded state is generally characterized as unstructured, but recent experiments have cast some doubt on this notion. Hou et al. (*44*) used two-dimensional NMR spectroscopy to identify regions that exhibit a clear preference for a β-strand conformation. Recent ECD, nuclear magnetic resonance (NMR), and vibrational spectroscopy studies provide conclusive evidence for the notion that the peptide exhibits a substantial fraction of amino acid residues adopting PPII (*39*, *45*−*47*). An analysis of the temperature dependence of the ECD spectra and the $^3J_{C\alpha HNH}$ coupling constants further revealed that the folding/unfolding process of the PPII contents of Aβ_{1-40} and of some of its fragments exhibits cooperativity (*39*).

The above-cited work on the amyloid β peptide and its fragments cast some doubt on the notion that longer peptide chains behave like a statistical coil, irrespective of their amino acid side-chain composition. To shed some further light on this important issue, it would be useful to study another peptide of comparable length, which is generally considered as unfolded and unstructured. Its amino acid sequence should be different from that of Aβ. The 32 amino acid polypeptide hormone calcitonin meets these requirements. It is produced by thyroidal C cells and forms amyloid fibrils with medullary carcinoma of the thyroid (*48*). Generally, calcitonin is a hormone peptide that inhibits osteoclastic bone resorption, induces calcium uptake from body fluids, and plays a role in calcium−phosphorus metabolism (*49*) The structure in aqueous solution is generally characterized as mostly random, but a helical structure is formed in the presence of methanol, trifluroethanol, and membrane-mimicking environments (*50*−*53*). Human (hCT) and salmon calcitonin (sCT) have a low sequence homology, and they have been shown to cause different amyloid-like fibrils (*48*, *54*, *55*). sCT, which is more effective in osteoclastic resorption inhibition than the human derivative (*52*), shows much slower fibrillation than hCT (*55*). We combined polarized Raman, FTIR, VCD, and ECD spectroscopy to explore the structural composition of unfolded sCT in water. Our investigations involved the calculation of the amide I′ profiles based on a structural model built by means of molecular mechanics calculations and by utilizing recently obtained structural propensities of amino acid residues in aqueous solution (*23*, *26*). The results are compared with those from a recent analysis of the amyloid β fragment, Aβ_{1-28}. This reveals clear structural differences that unambiguously show that peptides with different amino acid sequences can yield significant structural differences in the unfolded state. Our results are inconsistent with the concept that the unfolded state of peptides and proteins is independent of the respective amino acid sequence.

THEORETICAL BACKGROUND

The underlying theory of our spectral modeling has been described in detail in recently published papers (*56*). Briefly, we assume that the interaction between $N - 1$ amide I modes of a polypeptide containing N amino acid residues can be described in terms of a coupled oscillator model. The validity and applicability of the coupled oscillator model for describing the delocalized excited states in polypeptides have

recently been demonstrated by a variety of theoretical studies (*57*, *58*). The corresponding Hamiltonian is written as

$$\hat{H}_{ext} = \begin{pmatrix} \tilde{\nu}_1 & \Delta_{12} & \delta_{13} & \delta_{14} & \delta_{15} & \delta_{16} & . & . & . & 0 \\ \Delta_{21} & \tilde{\nu}_2 & \Delta_{23} & \delta_{24} & \delta_{25} & \delta_{26} & . & . & . & 0 \\ \delta_{31} & \Delta_{32} & \tilde{\nu}_3 & \Delta_{34} & \delta_{35} & \delta_{36} & \delta_{37} & . & . & 0 \\ \delta_{41} & \delta_{42} & \Delta_{43} & \tilde{\nu}_4 & \Delta_{45} & \delta_{46} & \delta_{47} & \delta_{48} & . & 0 \\ \delta_{51} & \delta_{52} & \delta_{53} & \Delta_{54} & . & . & . & . & . & . \\ \delta_{61} & \delta_{62} & \delta_{63} & \delta_{64} & . & . & . & . & & . \\ . & . & . & . & . & . & . & . & & . \\ . & . & . & . & . & . & . & . & . & \delta_{n-3,n-1} \\ 0 & . & . & . & . & . & . & . & \tilde{\nu}_{n-2} & \Delta_{n-2,n-1} \\ 0 & 0 & 0 & 0 & . & . & . & \delta_{n-1,n-3} & \Delta_{n-1,n-2} & \tilde{\nu}_{n-1} \end{pmatrix} \quad (1)$$

In our notation, we distinguish between nearest neighbor coupling, $\Delta_{j,j\pm1}$, and interactions between more distant residues, $\delta_{j,j'}$ ($j' = j \pm 2$, $j \pm 3$, and $j \pm 4$). The former involves through-bond as well as through-space coupling (*59*). Coupling parameter values were obtained from recent studies on tripeptides (*24*) and from results of *ab initio* and Density Functional Theory (DFT) calculations (*57*−*59*), whereas $\delta_{jj'}$ were assumed to predominantly result from transition dipole coupling (TDC). The corresponding eigenfunctions of the Schrödinger equation can be written as a linear combination of local oscillator functions. As a consequence, the Raman tensor as well as the transition dipole moment of an excitonic state can also be written as linear combinations of the Raman tensors and transition dipole moments of local amide I vibrations, respectively. To this end, the latter have to be transformed into a common coordinate system. This brings about an orientational dependence of IR and Raman scattering. The amide I band shapes can be calculated as a superposition of bands arising from the transitions into the $N - 1$ excitonic states.

The Raman tensor of the ith excitonic state, $\hat{\alpha}_i$, can be used to calculate the isotropic and anisotropic Raman intensities, which are proportional to the following isotropic and anisotropic tensor invariants (*60*)

$$\beta'^2_{\mathrm{iso},i} = \frac{1}{9}(Tr\hat{\alpha}'_i)^2$$

$$\gamma'^2_{\mathrm{aniso},i} = \frac{1}{2}[(\alpha'_{xx,i} - \alpha'_{yy,i})^2 + (\alpha'_{yy,i} - \alpha'_{zz,i})^2 + (\alpha'_{zz,i} - \alpha'_{xx,i})^2] + \frac{3}{4}[(\alpha'_{xy,i} + \alpha'_{yx,i})^2 + (\alpha'_{yz,i} + \alpha'_{zy,i})^2 + (\alpha'_{zx,i} + \alpha'_{xz,i})^2] \quad (2)$$

The integrated IR absorptivity ϵ_i^{IR} of the ith excitonic mode can be calculated by employing (*56*)

$$\epsilon_i^{\mathrm{IR}} = \varsigma \vec{\mu}_i \vec{\mu}_j \quad (3)$$

where $\vec{\mu}_i$ is the transition dipole moment of the amide I mode in units of esu cm, and

$$\varsigma = \frac{\tilde{\nu}_0}{n \cdot 9.2 \times 10^{-39}\ \mathrm{M\ esu^2\ cm^2}} \quad (4)$$

where $\tilde{\nu}_0$, the average amide I wavenumber, can be interpreted as the first moment of the entire IR band and n is the number of involved CO oscillators. ϵ_i^{IR} is expressed in units of $\mathrm{M^{-1}\ cm^{-1}}$ per residue.

The calculation of the VCD signal is somewhat less straightforward, in that it requires that, for a given oscillator, the magnetic moment induced by all of the remaining electric transition dipole moments is taken into account. This yields the expression for the rotational strength

$$R_i = \mathrm{Im}\left[\sum_{j=1}^{n-1} a_{ij}\vec{\mu}_j\left(\sum_{k=1}^{n-1} a_{ik}\vec{m}_k - \frac{i\pi}{2}\left(\sum_{l=1}^{n-2}\sum_{m=l}^{n-1} \tilde{\nu}_{lm}\vec{T}_{lm} \times (a_{il}\vec{u}_l - a_{im}\vec{u}_m)\right)\right)\right] \quad (5)$$

where $\vec{m}_k$ denotes the magnetic transition dipole moment associated with the local amide I mode of the kth residue, respectively. $\tilde{\nu}_{lm}$ is the average wavenumber of the two interacting modes associated with the lth and mth residues, and $\vec{T}_{lm}$ is the distance vector pointing from the lth to the mth residue. A similar expression has been obtained earlier by Xiang et al. (*61*).

The Raman, IR, and VCD amide I profiles can be calculated as a superposition of Gaussian bands representing the respective bands of the excitonic modes

$$I_{\mathrm{iso}}(\Omega) = \sum_{i=1}^{n-1}\left[\frac{{\beta_{s,i}}^2}{\sigma_i\sqrt{2\pi}} f(\Omega,\Omega_i)\right] \quad (6a)$$

$$I_{\mathrm{aniso}}(\Omega) = \sum_{i=1}^{n-1}\left[\frac{{\gamma_i}^2}{\sigma_i\sqrt{2\pi}} f(\Omega,\Omega_i)\right] \quad (6b)$$

$$\epsilon_{\mathrm{IR}}(\Omega) = \sum_{i=1}^{n-1}\left[\frac{\epsilon_i^{\mathrm{IR}}}{\sigma_i\sqrt{2\pi}} f(\Omega,\Omega_i)\right] \quad (6c)$$

$$\Delta\epsilon(\Omega) = \frac{\tilde{\nu}_0}{n \cdot 2.3 \times 10^{-39}\ \mathrm{M\ esu^2\ cm^2}} \sum_{i=1}^{n-1}\left[\frac{R_i f_i(\Omega,\Omega_i)}{\sigma_i\sqrt{\pi}}\right] \quad (6d)$$

where $f_i(\Omega,\Omega_i)$ denotes a set of Gaussian profiles centered at the eigenvalues Ω_i of the ith excitonic state.

MATERIALS AND METHODS

Materials. sCT ($M_w = 3431.9$, >99% purity) and $NaClO_4$ were purchased from Bachem (King of Prussia, PA) and Sigma−Aldrich Chemical Co. (St. Louis, MO), respectively. To remove residual TFA, which has a Raman band at ~1674 $\mathrm{cm^{-1}}$, the peptide was dialyzed at pH 1 using a 1 mL Spectra/Por CE Float A Lyzer dialysis bag with a MWCO of 500 and lyophilized overnight. IR, VCD, and ECD measurements were carried out at pD 5 and 13.5 (13.2 for ECD). An additional ECD spectrum was recorded at pD 1. Raman spectra were solely recorded for the alkaline sample. To adjust the desired pD value, the peptide was then dissolved

in D_2O, at a concentration of 25.0 mg/mL (0.007 M). After the addition of the peptide, the pD was adjusted to final values of 4.9 and 13.5 by adding small aliquots of DCl and NaOD (Acros Organics, Pittsburgh, PA), respectively.

Spectroscopies. Some preliminary Raman experiments at acidic and alkaline pD were performed in the Biospectroscopy Laboratory of the Department of Chemistry at the University of Puerto Rico, Río Piedras Campus. The set up is described in earlier publications (*24*). The final Raman spectra used for our analysis were obtained with the 442 nm (32 mW) excitation from a HeCd laser (Model IK 4601R-E, Kimmon Electric US). The laser beam was directed into a RM 100 Renishaw confocal Raman microscope and focused onto a 1.0 mm Q Silica cell with a thin glass cover slip with a $\times 50$ objective. The scattered light was filtered with a 442 nm notch filter, dispersed by a single-grating 1800 L/mm grating, and imaged onto a back-thinned Wright Instrument CCD. It was polarized by a combination of a linear polarizer and a $\lambda/2$ plate. The latter rotates the *y*-polarized light (perpendicular to the laser polarization) into the *x* direction to achieve an optimal spectrometer transmission. All spectra were recorded in the "continuous" mode for 300 s and stored on a PC for further spectral analysis. The peptide and the appropriate reference were measured a total of 4 times for each of the polarization directions, and the spectra were averaged to eliminate some of the noise. The reference spectra were appropriately subtracted from the sample spectra.

The FTIR and VCD spectra were recorded with a Chiral IR Fourier Transform VCD spectrometer from Bio Tools. The sample was placed into a cell with a path length of 50 μm. The spectral resolution was 8 cm^{-1} for both spectra. The VCD and IR were both collected as one measurement for a combined total time of 720 min. To eliminate any background and solvent contributions to the IR spectrum, the cell was first filled with the reference solvent, D_2O (pD 13.5), and was automatically subtracted by the ChiralIR software.

The UV ECD spectra in the wavelength range of 190−240 nm of sCT were measured with a JASCO J-810 spectrapolarimeter in a 0.1 mm quartz cell with 0.05 nm resolution, at the Drexel University Medical School. The peptides were dissolved in D_2O at a concentration of 10 mM. We performed the measurements in D_2O rather than in H_2O to allow for a comparison with structural data obtained by virtue of vibrational spectroscopies. As recently shown, the PPII propensity of, e.g., alanine is higher in H_2O than in D_2O (*25*). The samples were placed in a nitrogen-purged JASCO CD module. The temperature at the cuvette was controlled by means of a Peltier-type heating system (accuracy of ± 1 °C). For each measurement, the sample was allowed to equilibrate for 5 min at the adjusted temperature prior to acquisition. The spectra were obtained by averaging 10 scans and were collected as ellipticity as a function of the wavelength and converted to molar absorptivities via the equation

$$\Delta\epsilon = \frac{\theta}{32\,980 lcn} \tag{7}$$

where θ is the ellipticity in millidegrees, l is the path length of the cuvette in centimeters, c is the concentration in molarity, and n is the number of residues. Earlier ECD spectra had been recorded with an OLIS DSM-10 UV/vis CD spectrophotometer as described by Eker et al. (*25*).

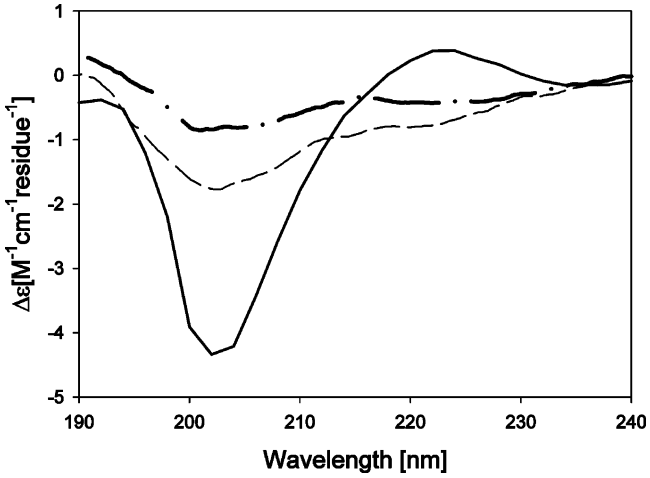

FIGURE 1: ECD spectra (in units of M^{-1} cm^{-1} per residue) of $A\beta_{1-28}$ (—) and sCT at pD 13.3 (- - -) and pD 5 (- · -), measured at 20 °C.

Spectral Analysis. All IR and Raman spectra were treated by using MULTIFIT (*62*). The calibration of the Raman spectrum was checked by using the D_2O band at 1207 cm^{-1}. To eliminate solvent contributions, we measured the solvent reference spectra for both polarizations, which were then subtracted from the corresponding peptide spectra. The isotropic and anisotropic Raman intensities were calculated as

$$I_{\text{iso}} = I_x - \frac{4}{3} I_y$$

$$I_{\text{aniso}} = I_y \tag{8}$$

where I_x and I_y denote the Raman scattering polarized parallel and perpendicular to the polarization of the exciting laser light.

Molecular Mechanics Calculations. We used the molecular mechanics program MMFF94 of the TITAN software package to obtain a possible conformation of the C-terminal cyclic N-terminal fragment CSNLSTC in explicit water (*63*). The program is an extension of the earlier published version of the Merck molecular force field (MMFF). MMFF94 was designed to facilitate the application to condensed-phase processes in MD simulations. It is described as a combined "organic/protein" force field that is equally applicable to proteins and other systems of biological significance. The core portion of MMFF94 is based on high-quality computational data for ca. 500 molecular structures optimized at the HF/6-31G* level, 475 structures optimized at the MP2/6-31G* level, 380 MP2/6-31G* structures evaluated at a defined approximation to the MP4SDQ/TZP level, and 1450 structures partly derived from MP2/6-31G* geometries and evaluated at the MP2/TZP level (*63*).

RESULTS AND DISCUSSION

Figure 1 depicts the ECD spectra of sCT measured at pD 5 and 13.3. The two pD values represent the protonated and deprotonated states of the alkaline side chains in sCT (K and R), which are the most likely source of any possible pH

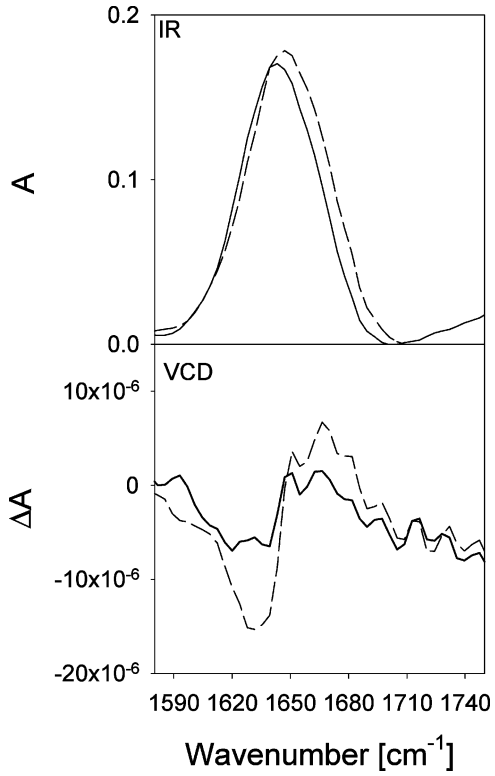

FIGURE 2: FTIR and VCD spectra of sCT in D_2O measured at pD 4.9 (- - -) and pD 13.6.

dependence of the peptide's structure. The recorded spectra are qualitatively similar, in that they depict two negative signals, a very large one at 205 nm and a small one between 220 and 230 nm, but the larger minimum is less pronounced in the spectrum measured at alkaline pD. The spectra agree well with that reported by Arvinte and Drake (*52*). We also measured the ECD spectrum at pD 1 and found it to be very similar to that recorded at pD 5 (data not shown).

The strong negative signal in the above ECD spectra is generally interpreted as reflecting a substantial PPII contribution to the conformational mixture (*25*, *27*, *29*). However, a classical PPII signal depicts a small but significant positive signal around 216 nm, which in our spectra is replaced by the above-mentioned small negative signal. Such a PPII-type spectrum was earlier recorded for the β-amyloid fragment Aβ_{1-28} (shown in Figure 1). A comparison with the basis spectra of Seerama and Woody (*64*) led us to conclude that the observed spectra reflect a mixture of PPII, short α-helix fragments, and β-strand-like conformations (β_s). The N-terminal loop caused by the disulfide bridge between C1 and C2 is also likely to provide a minor contribution to the ECD spectrum. The difference between the spectra taken at different pD values suggests that the PPII fraction is somewhat larger at the lower pD.

The amide I′ region of the FTIR spectra of sCT measured at pD 5 and 13.6 are displayed in Figure 2. The IR band profiles are very similar, but the amide I′ band of the pD 5 sample appears somewhat more asymmetric, in that it is slightly more intense on its high wavenumber side. We also measured the amide I′ band of acidic (pD 1) sCT and found it to be indistinguishable from that measured at pD 5 (data not shown). As we show below, the small difference between the amide I band profiles in Figure 2 is indicative of a slightly higher PPII population. This notion is consistent with the corresponding VCD profiles of amide I′, which are also displayed in Figure 2. For both pD values, the VCD signal can barely be discriminated from noise, but a slightly more pronounced minimum appears in the spectrum taken at pD 5.

The recording of polarized Raman spectra of sCT turned out to be much more challenging. The spectra taken at acidic pD and particularly those recorded at neutral pD were contaminated by a high fluorescence background, which deteriorated the signal-to-noise ratio especially of the anisotropic Raman spectra. Only the spectra recorded at alkaline pD were of sufficient quality to be useable for the more detailed structure analysis described below. Therefore, in the following, we confine ourselves on modeling the amide I′ band profiles of the Raman, IR, and VCD spectra recorded at alkaline pD (Figure 3). In fact, the alkaline state is also likely to be the more interesting, owing to the more pronounced difference between its ECD spectra and that of acidic Aβ_{1-28}. We reiterate in this context our specific aim to show that unfolded states of long peptides can be different, thus reflecting different intrinsic propensities of the respective amino acid residues.

In what follows, we describe the modeling of the amide I′ band profiles in terms of a structural model derived from molecular mechanics calculations, the ECD spectra in Figure 1, and individual conformational propensities of amino acid residues in unfolded peptides reported in the literature (*27*−*29*). We used our MULTIFIT program to isolate the amide I′ band profiles in the IR and Raman spectra. Moreover, we employed the Savitzky−Golay subprogram of MULTIFIT for a moderate smoothing of the Raman spectra. Care has been taken to avoid any deterioration of the band profile by the smoothing procedure. The result of this procedure is shown in Figure 3, which reveals a large noncoincidence of $\Omega_{IR} - \Omega_{iso} = 27$ cm^{-1} between the peak positions of the highly asymmetric IR and isotropic Raman bands, which is large compared with values recently obtained for *trans*-polyproline (13 cm^{-1}), $(AAKA)_2$ (18 cm^{-1}), and even Aβ_{1-28} (20 cm^{-1}). This indicates substantial contributions from conformers with strong excitonic coupling between adjacent amide I′ modes and a predominant conformational sampling in the upper left quadrant of the Ramachandran plot (*59*). Even more informative is the ratio

$$\xi_{aniso} = \frac{\Omega_{aniso} - \Omega_{IR}}{\Omega_{iso} - \Omega_{IR}} \qquad (9)$$

which reflects the position of the conformationally sensitive anisotropic Raman band between the peak positions of IR and isotropic Raman (*56*). For sCT, we obtained 0.33, which is comparable with the 0.31 value obtained for $(AAKA)_2$, (*65*) but it is much smaller than the corresponding values for polyproline (0.61) (*66*) and Aβ_{1-28} (0.5−0.6) (*46*). In the presence of a significant positive noncoincidence between IR and isotropic Raman scattering, values in the 0.5−0.6 range are indicative of a predominant PPII conformation, while smaller values reflect a substantial population of a more β-strand-like conformation (*65*). Thus, this first analysis already suggests that sCT is different from the earlier investigated (acidic) Aβ_{1-28}, in that it exhibits a larger β-strand population, in accordance with the corresponding ECD spectra in Figure 1. Additionally, Figure 4 compares

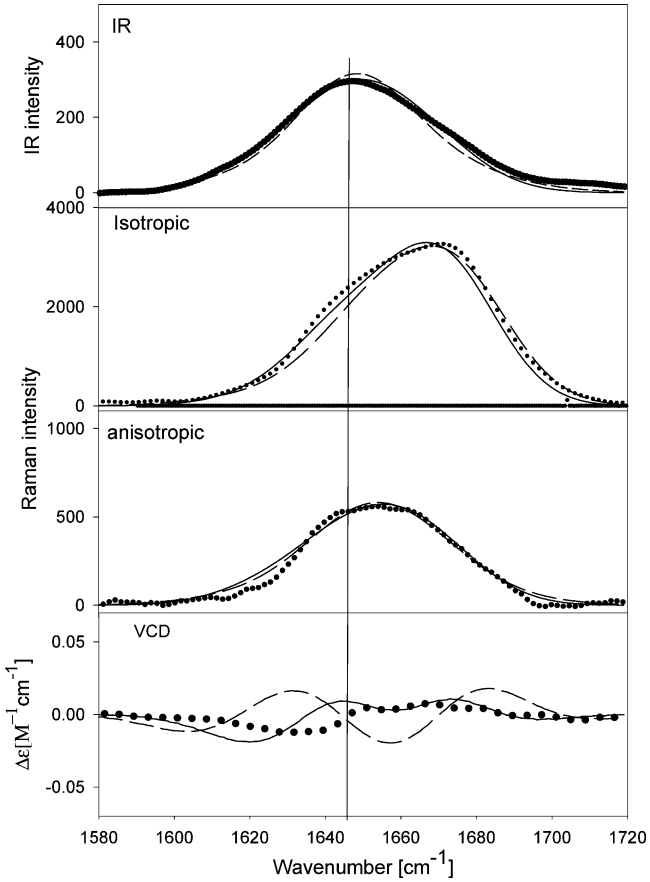

FIGURE 3: Amide I′ band profiles isolated from the isotropic and anisotropic Raman, IR, and VCD spectra of sCT measured at pD 13.5. The IR and VCD spectra are displayed in units of M^{-1} cm^{-1} per residue. The solid and dashed lines result from a simulation based on structural models M1 and M2 as described in the Results and Discussion.

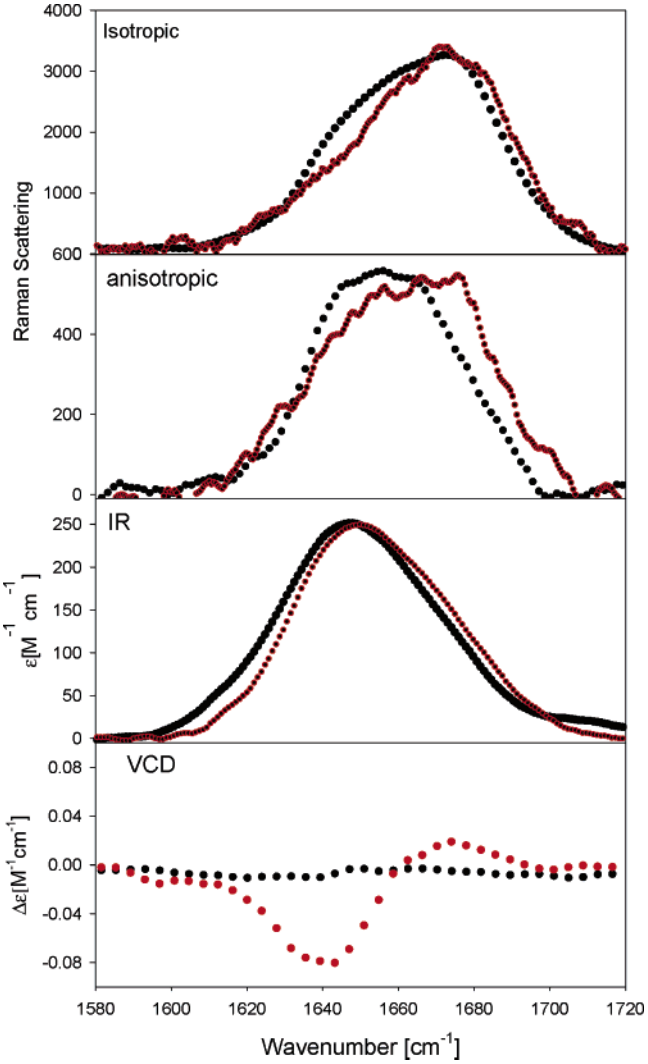

FIGURE 4: Comparison of the isotropic Raman, anisotropic Raman, FTIR, and VCD band profiles of amide I′ in the spectrum of sCT (measured at pD 13.5) and Aβ_{1-28} (measured at pD 1). The IR and VCD spectra are displayed in units of M^{-1} cm^{-1} per residue to allow for a quantitative comparison.

the IR, isotropic Raman, anisotropic Raman, and VCD spectra of alkaline sCT and acidic Aβ_{1-28}. Qualitative differences are discernible particularly for the anisotropic Raman profile and the VCD signal. In contrast to sCT, Aβ_{1-28} exhibits a very pronounced negative amide I couplet in the VCD spectrum, which is diagnostic of significant PPII contents (*15*). It should be mentioned in this context that the ECD spectrum of alkaline Aβ_{1-28} cannot be utilized for a comparison because it indicates a predominant α-helical conformation (Hagarman, Eker, Griebenow, Schweitzer-Stenner, unpublished results).

The above qualitative analysis already provides substantial evidence for the notion that the two naturally unfolded peptides Aβ_{1-28} and sCT differ significantly in terms of their structural composition. This is an important result in view of the fact that statistical coil models such as that utilized by Tran et al. predict that individual propensities become irrelevant for long polypeptides and proteins (*12*). Apparently, this seems not to be the case for sCT and Aβ_{1-28}.

To perform a more quantitative analysis based on our excitonic coupling model for amide I′, a suitable structural model for the N-terminal loop region, caused by the disulfide bridge between cysteines at positions 1 and 7, had to be obtained. We performed a conformational search for the cyclic N-terminal fragment CSNLSTC in explicit water by using the molecular mechanics software MMFF of the TITAN software package described above (*63*). To this end, we constructed a hydration shell for the initial structure, which had three water molecules in contact with a peptide linkage (two for hydrogen bonding to the carbonyl oxygen and one for accepting hydrogen bonding from the respective NH group).

The dihedral angles of the obtained lowest energy loop conformation are listed in Table 1. A conformation at only slightly higher energies was found to exhibit very similar dihedral angles. The next conformation in the energy hierarchy was obtained at ca. 3 kJ/mol higher in energy. Further conformations are associated with even higher energies. We performed calculations for different initial configurations of the hydration shell and obtained different structures from the optimization process. However, this ambiguity is not particularly cumbersome for our analysis, because the different optimized conformations just differed in terms of the sequence of the individual residue conformations rather than in the absolute values of the corresponding dihedral angles. Because the dominant contribution to excitonic coupling between amide I′ modes is provided predominantly by nearest neighbor coupling for all of the observed residue conformations, the IR and Raman band

Table 1

Dihedral Angles Obtained for the N-Terminal Loop of Salmon Calcitonin as Obtained from a Conformational Search with a Molecular Mechanics Calculation

(a)	C	S	N	L	S	T	C
ϕ (deg)	134.83	−70.8	−71.6	67.0	67.0	−87.5	−74.9
ψ (deg)		−13.6	−61.8	27.1	19.8	−31.9	−54.7

Structural Composition of the Segment V7−T32 of sCT Sequences Assumed for the Models M2 and M3 Described in the Results and Discussion (P, PPII; β, β-Strand-like Conformations)[a]

(b)	V	L	G	K	L	S	Q	Q	L	H	K	L	Q	T	Y	P	R	T	N	T	G	S	G	T
M2S1	β	P	P	P	P	P	P	P	P	β	P	P	P	β	P	P	P	β	P	β	P	P	β	β
M2S2	β	β	β	β	β	β	P	P	P	β	β	P	P	β	P	P	β	β	β	β	β	β	β	β
M2S3	β	α	α	α	α	α	α	α	α	α	α	α	α	β	P	P	β	β	β	β	β	β	β	β
M3S1	β	α	α	α	α	β	P	P	β	β	β	P	P	β	P	P	β	β	P	β	β	β	P	β
M3S2	β	β	β	α	α	α	α	P	β	β	β	P	P	β	P	P	β	β	P	β	β	β	P	β
M3S3	β	β	β	P	P	β	α	α	α	α	β	P	P	β	P	P	β	β	P	β	β	β	P	β
M3S4	β	β	β	P	P	β	P	P	β	β	β	P	P	β	P	P	β	β	P	β	β	β	P	β

[a] Simulations based on these two models yielded the profiles displayed by dashed and solid lines in Figure 3.

profiles of the different conformations are in fact very similar. Only the VCD signal does to some extent depend upon the sequence of the residue conformations. However, the C-terminal loop accounts only for 19% of the entire peptide, so that this uncertainty appears tolerable.

Our excitonic coupling model was parametrized by utilizing experimental and theoretical information from earlier studies. First, we estimated the intrinsic amide I′ wavenumber for the different residues, *j*, constituting the primary sequence of sCT by employing the relationship

$$\Omega_x = \Omega_A^{PPII} + \Delta\Omega_{Ax} + \Delta\Omega_{xy} \qquad (10)$$

where Ω_A^{PPII} is the local amide I′ wavenumber observed for the central peptide group in tetraalanine (*36*). $\Delta\Omega_{Ax}$ is the recently obtained difference between the amide I′ wavenumber of AA and the respective XA dipeptide, where X represents the set of considered amino acid residues (*47*). It reflects the direct side-chain dependence of the amide I wavenumber. $\Delta\Omega_{xy}$ is an additional shift reflecting the influence of the residue side chain (Y), which is the nearest neighbor toward the C-terminal (*47*). Second, we used ref *47* to obtain the individual electronic transition dipole strengths and (relative) Raman tensor elements of the amide I modes. The conformational dependence of the local amide I′ wavenumbers has been taken into account by using the contour maps of the diglycine peptide as reported by Gorbunov et al. (*58*). The loop conformation obtained from the above-described optimization procedure indicates that the peptide carbonyls of residues S2 and T6 are hydrogen-bonded to the backbone amides of C1 and C7. We took this into consideration by allowing an individual upshift of 10 cm^{-1} for the corresponding amide I′ modes, which accounts for the fact that such hydrogen bonds are likely to be weaker than hydrogen bonds between D_2O and the carbonyl group (*67*).

To construct a suitable structural model for the "unfolded" part of the peptide, we made use of the fact that the ECD spectrum suggests a mixture of PPII, β-strand, and a smaller α-helical conformation. The helical contribution is also discernible from the isotropic Raman and the FTIR band profiles of amide I, in that the low wavenumber shoulder in the isotropic Raman profile coincides with the peak wavenumber in the IR and the low wavenumber edge of the very broad profile of anisotropic Raman scattering. This shoulder is absent in the corresponding isotropic Raman profile of acidic Aβ_{1-28} (Figure 4). Simulations of amide I profiles have recently shown that the peak wavenumber of the Raman and IR profiles do not significantly differ for an α-helical conformation (*56*). Moreover, it is known that hydrated α-helices give rise to a downshifted amide I′ wavenumber (*68*), a notion corroborated by the FTIR spectrum of the predominantly helical alkaline Aβ_{1-28}, in which the amide I′ band appears at 1642 cm^{-1}, whereas it peaks at 1649 cm^{-1} in the spectrum of the PPII-dominated peptide at acidic pH (Eker, Griebenow, Schweitzer-Stenner, unpublished results). Earlier work on sCT in a helix-promoting environment suggests that the detected helical fraction is assignable to the L9−F19 region of the peptide (*51*, *53*). For non helical residues we assume either a PPII or a β_s conformation. For the latter, we invoked an antiparallel β-strand-like conformation (ϕ, ψ) = (−140°, 140°), an amide I′ downshift of 8 cm^{-1}, in accordance with the computational results of Gorbunov et al. (*58*), and a nearest neighbor coupling of 3.5 cm^{-1}, observed for the β_s peptide trivaline (*24*). Apparently, this cannot account for the very large noncoincidence between IR and isotropic Raman, which suggests a coupling value that is even somewhat larger than the 5.0−6.5 cm^{-1} obtained for PPII (*58*). Different *ab initio* calculations for short peptides agree in predicting that even modest changes of ψ and ϕ can significantly increase nearest neighbor coupling between amide I modes in the vicinity of the canonical PPII conformation (*58*, *59*). We used a coupling constant of 10 cm^{-1}, corresponding to a slightly deformed PPII conformation (ϕ, ψ) = (−70°, 150°).

The first model (M1) employed was a rather crude and physically very unlikely "all or nothing" model for the unfolded state (*69*), i.e., the coexistence of chains for which residues 7−32 are all either in the PPII or in the β-strand conformation. Additionally, we considered a conformation for which segments 9−10 were helical and the remaining ones were either all PPII or β_s. We performed this simulation for various mixings of these two species. Even for the best case, i.e., a 40(PPII)/40(β_s)/20(α) % mixture, the agreement with the anisotropic Raman and IR band profiles was modest, whereas a much too large negative VCD couplet was calculated. Moreover, we could not adequately reproduce the asymmetry of the isotropic Raman band.

The second model (M2) is a much more likely scenario, in that we utilized the conformational propensities of amino acid residues, which we and others obtained from studies on short peptides, mostly in an alanine or proline context (*26*, *28*). We built three different representative sequences of residue conformations, described as follows. For sequence 1 (M2S1), we assumed that only residues with an unambiguous β propensity (V, H, and T) adopt a β-strand conformation, while the remaining residues were assumed to be PPII. On the contrary, sequence 2 (M2S2) is mostly β-strand with the exception of L, Q, E, and P, which adopt PPII. Additionally, we assumed that the conformation of Y is PPII because P is its right neighbor (*28*). Sequence 3 (M2S3) contains a helical segment encompassing residues 9−19. The remaining part is mostly β-strand with some PPII admixtures. All sequences are listed in Table 1. This model assumes that a substantial persistence length for PPII and β_s is possible, in line with MD results for alanine (*40*−*43*), but at variance with the statistical model of Tran et al. (*12*) and Jha et al. (*13*). Because a recent NMR experiment revealed a substantial population of the cis conformation of P21, we assumed a 35:65 mixture of *cis* and *trans* proline for both conformers (*51*). The remaining part is mostly β-strand. The band profiles of this ensemble were calculated for different M2S1/M2S2/M2S3 mixing ratios. This yielded a reasonable reproduction of all spectra as visualized by the dashed lines in Figure 3. The VCD appears significantly reduced because of opposing contributions from the considered conformers. However, the rotational strength is still somewhat overestimated, and the form of the negative couplet is not reproduced. However, in view of the fact that the considered conformers still represent a more complex mixture, even the VCD simulation appears satisfactory. The ratio for an optimal simulation was M2S1/M2S2/M2S3 = 0.4:0.45:0.15. Thus, about 44% of the nonloop residues adopt PPII; 49% adopt β-strand; and 7% adopt an α-helical conformation. An analysis of the simulation reveals that the high wavenumber asymmetry of the IR profile results from the loop contribution, whereas the low wavenumber asymmetry of the isotropic Raman band and the particularly low wavenumber of the IR peak wavenumber result from the helical conformer. The very broad anisotropic Raman band just results from the different positions of all of the conformers considered in our simulation.

The third model (M3) assumes a shorter persistence length for PPII and β_s. It comprises four sequences, three of which (M3S1−M3S3) contain short, 4-residue α-helical segments. The remaining, unfolded part of the peptide and the helix-free sequence M3S4 can be considered as representing a typical member of a statistical coil ensemble. The maximal persistence length is 2 residues for PPII and 3 residues for β_s. The somewhat higher weighting of β_s reflects the significant fraction of residues that exhibit a clear β_s preference in the unfolded state, namely, V, T, S, and H (*26*−*28*, *70*). Even though M3S1−M3S4 represents only four of numerous statistical coil ensembles (in the absence of any persistence length supporting nonlocal interactions), they can be considered to be representative with respect to their nonhelical part, because our spectroscopic method probes mostly the local environment of a given residue encompassing the two nearest neighbors on its N- and C-terminal side, owing to the predominance of nearest neighbor excitonic coupling in extended conformations (*59*, *71*). We assumed a coexistence between short helical segments rather than a single longer helix to account for the weak α-helix signal in the ECD spectrum. It is known that it becomes disproportionately weak for short helices, owing to the long-range electronic interactions governing the ECD spectrum of α-helices (*72*). We did not distinguish between *cis* and *trans* conformations of P24 because we found a limited influence on the band profiles of the four considered sequences. The simulation based on this model is visualized by solid lines in Figure 3. It was calculated with fractions 0.35 (M3S1), 0.26 (M3S2), 0.33 (M3S3), and 0.07 (M3S4). The reproduction of the IR and Raman band profiles is very satisfactory. In comparison with the simulation based on the M2 model, this modeling reproduces the IR and the isotropic Raman profile slightly better (particularly the α-helix contribution in the latter) than that achieved by M2 and is even more successful in reducing the VCD signal close to the observed values. This is a particularly important and, by far, nontrivial achievement. Our simulation suggests that the weak rotational strength of amide I′ reflects a compensation of the negative PPII and the positive α-helical couplet. The former is already less intense than, e.g., the corresponding contribution in Aβ_{1-28}, owing to the different PPII fractions (0.43 for sCT and 0.65 for Aβ_{1-28}).

The small differences between the VCD and IR spectra of alkaline and neutral sCT can be explained by a slightly larger PPII content in the latter. This can be understood by assuming that the two lysine residues have a higher PPII propensity in the protonated state. In fact, this has been shown by Rucker and Creamer (*22*). The absence of any pH dependence in the acidic region reflects the absence of any residue with a carboxylate side chain in the peptide sequence. This distinguishes it from many unfolded proteins and peptides that show an above average fraction of glutamic acid residues (*2*).

The results of our simulation confirm the notion inferred from a qualitative analysis of the measured ECD and vibrational spectra that sCT contains less PPII and more β_s than Aβ_{1-28}. Thus, they confirm the validity of the experimentally obtained conformational propensities of amino acid residues (*26*−*28*, *70*) and demonstrate that they still matter even for longer peptides. This is somewhat at variance with predictions of Tran et al. (*12*). This discrepancy is due to the lesser differences between conformational propensities of, e.g., Q, L, K, T, and V, resulting from their calculations. Our results further suggest that the "unfolded" part of sCT may indeed exhibit a statistical coil. The recent study of Danielsson et al. (*39*) suggests that this is not the case for Aβ_{1-28}. This does not only concern side chains with PPII propensity but also those with a strong preference of β_s. Results reported by Danielsson et al. (*39*) and Hou et al. (*44*) suggest that, e.g., the hydrophobic segment containing the VFF motif is entirely in a β_s-like conformation. The latter data further suggest a relatively large persistence length for β_s or a β_s-like conformation in the C-terminal, hydrophobic Aβ_{30-42}, which again reflects the high β propensity of the involved amino acid residues.

As mentioned before, sCT is not very effective and comparatively slow in aggregating into fibrils, in contrast to Aβ_{1-28} (*54*, *55*). This seems to be consistent with the hypothesis that peptides/proteins with a large PPII content

are more likely to form aggregates. Blanch et al. (*20*) argued that the PPII → β-sheet transition would be entropically more favorable than a coil → β-sheet transition, owing to the elimination of the comparatively ordered water molecules stabilizing PPII (*73*). However, a high PPII propensity is certainly not a sufficient condition for aggregation. This has been demonstrated by Syme et al. (*21*) by showing that the β-fibril formation of α-, β-, and γ-synuclein is substantially different, even though their respective PPII content is similar. This led the authors to conclude that the low net charges and high hydrophobicity are at least of equal importance (*74*).

REFERENCES

1. Anfinsen, C. B., Haber, E., Sela, M., and White, F. N. (1961) Kinetics of formation of native ribonuclease during oxidation of the reduced polypeptide chain, *Proc. Natl. Acad Sci. U.S.A. 47*, 1309−1314.
2. Dunker, A. K., Lawson, J. D., Brown, C. J., Williams, R. M., Romero, P., Oh, J. S., Oldfield, C. J., Campen, A. M., Ratliff, C. M., Hipps, K. W., Ausio, J., Nissen, M. S., Reeves, R., Kang, C., Kissinger, C. R., Bailey, R. W., Griswold, M. D., Chiu, W., Garner, E. C., and Obradovic, Z. (2001) Intrinsically disordered protein, *J. Mol. Graphics Modell. 19*, 26−59.
3. Tompa, P. (2002) Intrinsically unstructured proteins, *Trends Biochem. Sci. 27*, 527.
4. Glenner, G. C., and Wong, C. W. (1984) Alzheimer's disease and Down's syndrome−Sharing of a unique cerebrovascular amyloid fibril protein, *Biochem. Biophys. Res. Commun. 120*, 885−890.
5. Masters, C. L., Multhaupt, G., Simms, G., Pottgieser, J., Martins, R. N., and Beyreuther, K. (1985) Neuronal origin of a cerebral amyloid: Neurofibrillary tangles of Alzheimer's disease contain the same protein as the amyloid of plaque cores and blood vessels, *EMBO J. 4*, 2757−2763.
6. Lee, G. M.-Y., Balin, B. J., Otvos, L., and Trojanowski, J. Q. (1991) A68: A major subunit of paired helical filaments and derivatized forms of normal tau, *Science 251*, 675−678.
7. Arawaka, S., Saito, Y., Murayama, S., and Mori, M. (1998) *Neurology 51*, 887−889.
8. Jha, A. K., Colubri, A., Zaman, M. H., Koide, S., Sosnick, T. R., and Freed, K. F. (2005) Helix, sheet, and polyproline II frequencies and strong nearest neighbor effects in a restricted coil library, *Biochemistry 44*, 9691−9702.
9. Flory, P. J. (1969) *Statistical Mechanics of Chain Molecules*, pp 30−31, Wiley and Sons, New York.
10. Brant, D. A., and Flory, P. J. (1965) The configuration of random polypeptide chains. 2. Theory, *J. Am.. Chem. Soc. 87*, 2791−2800.
11. Kohn, J. E., Millett, I. S., Jacob, J., Zagrovic, B., Dillon, T. M., Cingel, N., Dothager, R. S., Seifert, S., Thiyagarajan, P., Sosnick, T. R., Hasan, M. Z., Pande, V. S., Ruczinski, I., Doinach, S., and Plaxco, K. W. (2004) Random-coil behavior and the dimensions of chemically unfolded proteins, *Proc. Natl. Acad. Sci. U.S.A. 101*, 12491−12496.
12. Tran, H. T., Wang, X., and Pappu, R. V. (2005) Reconciling observations of sequence-specific conformational propensities with the generic polymeric behavior of denatured proteins, *Biochemistry 44*, 11369−11380.
13. Jha, A. K., Colubri, A., Freed, K. F., and Sosnick, T. R. (2005) Statistical coil model of the unfolded state: Resolving the reconciliation problem, *Proc. Natl. Acad. Sci. U.S.A. 102*, 13099−13104.
14. Tiffany, M. L., and Krimm, S. (1968) New chain conformations of poly(glutamic acid) and polylysine, *Biopolymers 6*, 1767−1770.
15. Dukor, R., and Keiderling, T. (1991) Reassessment of the random coil conformation: Vibrational CD study of proline oligopeptides and related polypeptides, *Biopolymers 31*, 1747−1761.
16. Keiderling, T. A., and Xu, Q. (2002) Unfolded proteins studied with IR and VCD spectra, *Adv. Protein Chem. 62*, 111−161.
17. Cowan, P. M., and McGavin, S. (1955) Structure of poly-L-proline, *Nature 176*, 501.
18. Shi, Z., Woody, R. W., and Kallenbach, N. R. (2002) Is polyproline II a major backbone conformation in unfolded proteins? *Adv. Protein Chem. 62*, 163−240.
19. Chang, J.-F.; Phillips, K.; Lundbäck, T.; Gstaiger, M.; Ladbury, J. E., and Luisi, B. (1999) Oct-1 POU and octamer DNA co-operate to recognise the Bob-1 transcription co-activator via induced folding, *J. Mol. Biol. 288*, 941−952.
20. Blanch, E. W., Morozowa-Roche, L. A., Cochran, D. A. E., Doig, A. J., Hecht, L., and Barron, L. D. (2000) Is polyproline II helix the killer conformation? A Raman optical activity study of the amyloidogenic prefibrillar intermediate of human lysozyme, *J. Mol. Biol. 301*, 553−563.
21. Syme, C. D., Blanch, E. W., Holt, C., Ross, J., Goedert, M., Hecht, L., and Barron, L. D. (2002) A Raman optical activity study of rheomorphism in caseins, synucleins and tau, *Eur. J. Biochem. 269*, 148−156.
22. Rucker, A. L., and Creamer, T. P. (2002) Polyproline II helical structure in protein unfolded states: Lysine peptides revisited, *Protein Sci. 11*, 980−985.
23. Woutersen, S., and Hamm, P. (2000) Structure determination of trialanine in water using polarized sensitive two-dimensional vibrational spectroscopy, *J. Phys. Chem. B 104*, 11316−11320.
24. Eker, F., Cao, X., Nafie, L., and Schweitzer-Stenner, R. (2002) Tripeptides adopt stable structures in water. A combined polarized visible Raman, FTIR and VCD spectroscopy study, *J. Am. Chem. Soc. 124*, 14330−14341.
25. Eker, F., Griebenow, K., and Schweitzer-Stenner, R. (2003) Stable conformations of tripeptides in aqueous solution studied by UV circular dichroism spectroscopy, *J. Am. Chem. Soc. 125*, 8178−8185.
26. Eker, F., Griebenow, K., Cao, X., Nafie, L., and Schweitzer-Stenner, R. (2004) Preferred backbone conformations in the unfolded state revealed by the structure analysis of alanine based (AXA) tripeptides in solution, *Proc. Natl. Acad. Sci. U.S.A. 101*, 10054−10059.
27. Chen, K., Liu, Z., and Kallenbach, N. R. (2004) The polyproline II conformation in short alanine peptides is noncooperative, *Proc. Natl. Acad. Sci. U.S.A. 15*, 101, 15351.
28. Chellgren, B. W., and Creamer, T. P. (2004) Short sequences of non-proline residues can adopt the polyproline II helical conformation, *Biochemistry 43*, 5864−5869.
29. Chen, K., Liu, Z., Zhou, C., Shi, Z., and Kallenbach, N. R. (2005) Neighbor effect on PPII conformation in alanine peptides, *J. Am. Chem. Soc. 127*, 10146−10147.
30. Eker, F., Griebenow, K., Cao, X., Nafie, L., and Schweitzer-Stenner, R. (2004) Tripeptides with ionizable side chains adopt a perturbed polyproline II structure in water, *Biochemistry 43*, 613−621.
31. Shi, Z., Olson, C. A., Rose, G. A., Baldwin, R. L., and Kallenbach, N. R. (2002) Polyproline II structure in a sequence of seven alanine residues, *Proc. Natl. Acad. Sci. U.S.A. 99*, 9190.
32. Epand, R. M., and Scheraga, H. A. (1968) The influence of long-range interactions on the structure of myoglobin, *Biochemistry 7*, 2864−2872.
33. Wüthrich, K., and Gratewohl, C. (1974) A novel approach for studies of the molecular conformations in flexible polypeptides, *FEBS Lett. 43*, 337−340.
34. Zimmermann, S. S., Pottle, M. S., Nèmethy, G., and Scheraga, H. A. (1976) Conformational analysis of the 20 naturally occurring amino acid resiudes using ECEPP, *Macromolecules 9*, 408−416.
35. Kohn, J. E., Millet, I. S., Jaby, J., Zagrovic, B., Dillon, T. M., Cingal, N., Dothager, R. S., Seifert, S., Thiyagarajan, P., Sosnick, T. R., Hasan, M. Z., Pande, V. S., Ruczinski, I., Donaich, S., and Plaxco, K. W. (2004) Random-coil behavior and the dimensions of chemically unfolded proteins, *Proc. Natl. Acad. Sci. U.S.A. 101*, 12491−12496.
36. Schweitzer-Stenner, R., Eker, F., Griebenow, K., Cao, X., and Nafie, L. A. (2004) The conformation of tetraalanine in water determined by polarized Raman, FTIR and VCD spectroscopy, *J. Am. Chem. Soc. 126*, 2768−2776.
37. McColl, I. H., Blanch, E. W., Hecht, L., Kallenbach, N. R., and Barron, L. D. (2004) Vibrational Raman optical activity characterization of poly(L-proline II) helix in alanine oligopeptides, *J. Am. Chem. Soc. 126*, 5076−5077.
38. Ma, K., Kan, L.-s., and Wang, K. (2001) Polyproline II helix is a key structural motif of the elastic PEKV segment of titin, *Biochemistry 40*, 3427−3438.
39. Danielsson, J., Jarvet, J., Damberg, P., and Gräslund, A. (2005) The Alzheimer β-peptide shows temperature-dependent transitions between left-handed 3_1-helix, β-strand and random coil secondary structure, *FEBS J. 272*, 3938−3949.

40. Garcia, A. (2004) Characterization of non α-helical conformations in Ala peptides, *Polymers 45*, 669−676.
41. Kentsis, A., Mezei, M., Gindin, T., and Osman, R. (2004) Unfolded state of polyalanine is a segmented polyproline II helix, *Proteins 55*, 493−501.
42. Mezei, M.; Fleming, P. J., Srinivasam, R., and Rose, G. D. (2004) Polyproliine II helix is the preferred conformation for unfolded polyalanine in water, *Proteins 55*, 502−507.
43. Fleming, P. J., Ftzkee, N. C., Mezei, M. Y., Srinivasan, R., and Rose, G. D. (2005) A novel method reveals that solvent water favors polyproline II over β-strand conformation in peptides and unfolded proteins: Conditional hydrophobic accessible surface area (CHASA), *Proteins 14*, 111−118.
44. Hou, L., Shao, H., Zhang, Y., Li, H., Menon, N. K., Neuhaus, E. B., Brewer, J. M., Byeon, I.-J. L., Ray, D. G., Vitek, M. P., Iwashita, T., Makula, R. A., Przybyla, A. B., and Zagorski, M. Z. (2004) Peptides establish that the Met35 oxidation state affects the mechanism of amyloid formation, *J. Am. Chem. Soc. 162*, 1992−2005.
45. Jarvet, J., Damberg, P., Danielson, J., Johansson, I., Erikson, L. E., and Gräslund, A. (2003) A left-handed 31 helical conformation in the Alzheimer Aâ(12−28) peptide, *FEBS Lett. 555*, 371−374.
46. Eker, F., Griebenow, K., and Schweitzer-Stenner, R. (2004) Aβ_{1-28} fragment of the amyloid peptide predominantly adopts a polyproline II conformation in an acidic solution, *Biochemistry 43*, 6893−6898.
47. Measey, T., Hagarman, A., Eker, F., Griebenow, K., and Schweitzer-Stenner, R. (2005) Side chain dependence of intensity and wavenumber position of amide I′ in IR and visible Raman spectra of XA and AX dipeptides, *J. Phys. Chem. B 109*, 8195−8205.
48. Andreotti, G., and Motta, A. (2004) Modulating calcitonin fibrillogenesis: An antiparallel α-helical dimer inhibits fibrillation of salmon calcitonion, *J. Biol. Chem. 279*, 6364−6370.
49. Austin, L. A., and Heath, H., III (1981) Calcitonin: Physiology and pathophysiology, *N. Engl. J. Med. 304*, 296−278.
50. Epand, R. M., Epand, R. F., Orlowksi, R. C., Seyler, J. K., and Colescott, R. L. (1986) Conformational flexibility and biological activity of salmon cacitonin, *Biochemistry 25*, 1964−1968.
51. Amodeo, P., Morelli, M. A. C., and Motta, A. (1994) Multiple conformations and proline *cis* ↔ trans isomerization in salmon calcitonin: A combined nuclear magnetic resonance, distance geometry, and molecular mechanics study, *Biochemistry 33*, 10754−10762.
52. Arvinte, T., and Drake, A. F. (1993) Comparative study of human and salmon calcitonin secondary structure in solutions with low dielectric constants, *J. Biol. Chem. 268*, 6408−6414.
53. Amodeo, P., Motta, A., Strazzullo, G., and Morelli, M. A. C. (1999) Conformational flexibility in calcitonin: The dynamic properties of human and salmon calcitonin in solution, *J. Biomol. NMR 13*, 161−174.
54. Kamihira, M., Naito, A., Tuzi, S., Nosaka, A. Y., and Saito, H. (2000) Conformational transitions and fibrillation mechanism of human calcitonin as studied by high-resolution solid-state ^{13}C NMR, *Protein Sci. 9*, 867−877.
55. Kamihira, M., Oshiro Y., Tuzi, S., Nosaka, A. Y., Saito, H., and Naito, A (2003) Effect of electrostatic interaction on fibril formation of human calcitonin as studied by high-resolution solid state ^{13}C NMR, *J. Biol. Chem. 278*, 2859−2865.
56. Schweitzer-Stenner, R. (2004) Secondary structure analysis of polypeptides based on an excitonic coupling model to describe the band profile of amide I of IR, Raman, and vibrational circular dichroism spectra, *J. Phys. Chem. 108*, 16965−16975.
57. Ham, S., and Cho, M. (2003) Amide I modes in the *N*-methylacetamide dimer and glycine dipeptide analog: Diagonal force constants, *J. Chem. Phys. 118*, 6915−6922.
58. Gorbunov, R. D., Kosov, D. S., and Stock, G. (2005) *Ab initio*-based exciton model of amide I vibrations in peptides: Definition, conformational dependence, and transferability, *J. Chem. Phys. 122*, 224904, 1−12.
59. Torii, H., and Tasumi, M. (1998) *Ab initio* molecular orbital study of the amide I vibrational interactions between the peptide groups in di- and tripeptides and considerations on the conformation of the extended helix, *J. Raman Spectrosc. 29*, 81−86.
60. Long, D. A. (2002) *The Raman Effect. A Unified Treatment of the Theory of Raman Scattering by Molecules*. Wiley and Sons, New York.
61. Xiang, T., Goss, D. J., Diem, M. (1993). Strategies for the computation of infrared CD and absorption spectra of biological molecules: Ribonucleic acids, *Biophys. J. 65*, 1255.
62. Jentzen, W., Unger, E., Karvounis, G., Shelnutt, J. A., Dreybrodt, W., and Schweitzer-Stenner, R. (1996) Conformational properties of nickel(II) octaethylporphyrin in solution. 1. Resonance excitation profiles and temperature dependence of structure-sensitive Raman lines, *J. Phys. Chem. 100*, 14184−14191.
63. Halgren, J. (1995). Merck molecular force field: 1. Basics, form, scope, parameterization, and performance of MMFF94*, *J. Comput. Chem. 17*, 490−519.
64. Sreerama, N., and Woody, R. W. (1994) Poly(Pro)II helices in globular proteins: Identification and circular dichroic analysis, *Biochemistry 33*, 10022−10025.
65. Measey, T., and Schweitzer-Stenner, R. (2006) The conformations adopted by the octamer peptide $(AAKA)_2$ in aqueous solution probed by FTIR and polarized Raman spectroscopy, *J. Raman Spectrosc.* In press.
66. Measey, T., and Schweitzer-Stenner, R. (2005) Simulation of amide I′ band profiles of trans polyproline based on an excitonic coupling model, *Chem. Phys. Lett. 408*, 123−127.
67. Schweitzer-Stenner, R., Sieler, G., and Christiansen, H. (1998) Competition between peptide−peptide and peptide−solvent hydrogen bonding probed by polarized Raman spectroscopy on *N*′-methylacetamide, *Asian J. Phys. 7*, 287−312.
68. Callender, R. H., Dyer, R. B., Gilmanshire, R., and Woodruff, W. H. (1998) Fast events in protein folding, *Annu. Rev. Phys. Chem. 49*, 173−202.
69. Schellman, J. A. (1958) The factors affecting the stability of hydrogen-bonded polypeptide structures in solution, *J. Phys. Chem. 62*, 1485−1494.
70. Hagarman, A., Measey, T., Doddasomayajula, R. S., Dragomir, I., Eker, F., Griebenow, K., and Schweitzer-Stenner R. (2006) Conformational analysis of XA and AX dipeptides in water by electronic circular dichroism and ^{1}H NMR spectroscopy, *J. Phys. Chem. B*, in press.
71. Huang, Q., and Schweitzer-Stenner, R. (2004) Conformational analysis of tetrapeptides by exploiting the excitonic coupling between amide I modes, *J. Raman Spectrosc. 35*, 586−589.
72. Boyden, N. N., and Asher, S. A. (2001) UV Raman studies of peptide conformation demonstrate that betanova does not cooperatively unfold, *Biochemistry 40*, 13723−13727.
73. Mezei, M., Fleming, P. J., Srinivasan, R., and Rose, G. D. (2004) Polyproline II helix is the preferred conformation for unfolded polyalanine in water, *Proteins: Struct., Funct., Bioinf. 55*, 502−507.
74. Uversky, V. N. (2002) What does it mean to be natively unfolded? *Eur. J. Biochem. 269*, 2−12.

BI052282R